PHYSICAL MODELING FOR DYNAMIC CONTROL OF MELTING PROCESS IN DIRECT-SLS

S. Ahn, J. Murphy, J. Ramos, and J. J. Beaman
Department of Mechanical Engineering
The University of Texas at Austin, Austin TX 78712

Abstract

During the melting process by laser irradiation, it is essential to understand the phase change processes to get high quality Direct SLS parts especially when high-order scanning paths are needed. This process is a transient three-dimensional heat conduction problem with a moving heat source and a moving phase boundary. The process can be simplified to a one-dimensional moving boundary model using appropriate assumptions. To implement a real-time control strategy, approximate solutions were found using three methods. Experiments using a CW CO_2 laser were performed on low carbon steel samples to verify the models' results. By using first order differential equations derived from the model, multi-input multi-output (MIMO) control strategies can be applied.

Introduction

Laser fusion based SFF processes need a real time control strategy that incorporates melt depth information.[1] Direct-SLS processes involve accurate melting of powder layers and fusion bonding of that layer with the previously deposited layer. The current process lacks melt-depth control capability. Also when high-order scanning paths are needed, the power or speed of the laser beam must be adjusted along the path to provide sufficient depth of melt. Superheating of the liquid zone must be controlled because melting of the entire powder layer thickness and fusion bonding to the previously deposited layer is required. To understand this process, we need to know the temperature distribution inside the material and the melt depth information. To solve this temperature distribution and melt depth, one-dimensional heat conduction with appropriate assumptions have been used.[2-5]. Three different models were used to compare results with experimental data. Each model used slightly different solution methodology and assumptions.

Physical Models

Transient three-dimensional heat conduction with a moving heat source and a moving phase boundary as shown in Fig. 1 is described by the following general governing equations and boundary conditions. V_s and $S(X_s,Y_s,Z_s,t)$ are the heat source velocity and phase boundary surface, respectively.

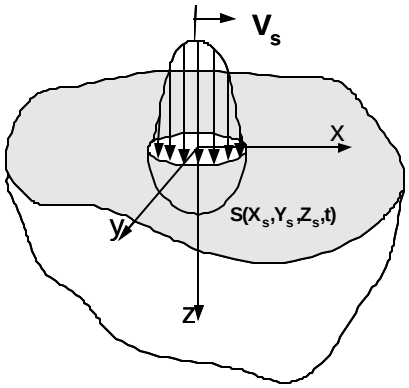

Figure 1: Schematic of a transient three-dimensional heat conduction with a moving heat source and moving phase boundary.

General Heat Diffusion Equation:

$$\frac{\partial}{\partial t}(rCT)+\vec{V}\cdot\nabla(rCT)=\nabla\cdot(k\nabla T) \qquad (1)$$

Equation 1 can be solved separately for the solid and liquid regions with the following boundary and interface conditions.

General Boundary Conditions:

$$-k_l\frac{\partial T}{\partial z}=es(T^4-T_\infty^4)+h_\infty(T-T_\infty)+q_{in} \quad \text{at } z=0 \qquad (2)$$

$$T=T_0 \text{ at } t=0 \qquad (3)$$

$$T=T_0 \text{ at } x\to\pm\infty \quad y\to\pm\infty \quad z\to\infty \qquad (4)$$

Phase Interface Conditions:

$$\left[1+\left(\frac{\partial X_s}{\partial y}\right)^2+\left(\frac{\partial X_s}{\partial z}\right)^2\right]\left(k_s\frac{\partial T_s}{\partial x}-k_l\frac{\partial T_l}{\partial x}\right)=L\left(\frac{\partial X_s}{\partial t}-V_x\right) \qquad (5a)$$

$$\left[1+\left(\frac{\partial Y_s}{\partial x}\right)^2+\left(\frac{\partial Y_s}{\partial z}\right)^2\right]\left(k_s\frac{\partial T_s}{\partial y}-k_l\frac{\partial T_l}{\partial y}\right)=L\left(\frac{\partial Y_s}{\partial t}-V_y\right) \qquad (5b)$$

$$\left[1+\left(\frac{\partial Z_s}{\partial x}\right)^2+\left(\frac{\partial Z_s}{\partial y}\right)^2\right]\left(k_s\frac{\partial T_s}{\partial z}-k_l\frac{\partial T_l}{\partial z}\right)=L\left(\frac{\partial Z_s}{\partial t}-V_z\right) \qquad (5c)$$

Here T, k_i, r, e, s, L, h¥ are temperature, thermal conductivity of ith phase, density, emissivity, Stefan-Boltzmann constant, latent heat of fusion, and convention coefficient, respectively. [9]

Assumptions

The general three-dimensional problem can be simplified to a one-dimensional moving boundary problem (e.g. Stefan problem) by using the following assumptions:

- Thermo-physical properties are considered independent of temperature and constant in space within each phase region.
- Velocity of moving beam is replaced by an equivalent interaction time, $\Delta t = \frac{D_b}{V_s}$ where D_b is beam diameter and V_s is scan speed. [13] (See Fig. 2)
- 1-D approximation is enough to predict the maximum depth of melt when the interaction time is less than the radial thermal diffusion time ($FourierNumber \equiv \frac{4a\Delta t}{D_b^2} \leq 1$, α is thermal diffusivity).
- Heat losses by radiation, convection and lateral conduction can be included in an overall absorption coefficient for the surface.

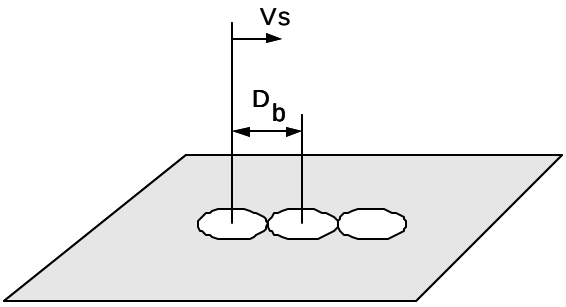

Figure 2: Illustration of interaction time.

Generalized 1-D Model

Using the above assumptions, the general governing equations can be simplified to the equations shown below. Figure 3a shows a cross section of the actual phase boundary. The maximum boundary depth is approximately uniform away from the edges and demonstrates a one-dimensional approximation is reasonable to predict maximum melt depth. Figure 3b shows a schematic of the 1-D model with model parameters included. *I, A, z_m,* and *d* are laser intensity, absorption coefficient, melt depth, and thermal boundary layer thickness, respectively.

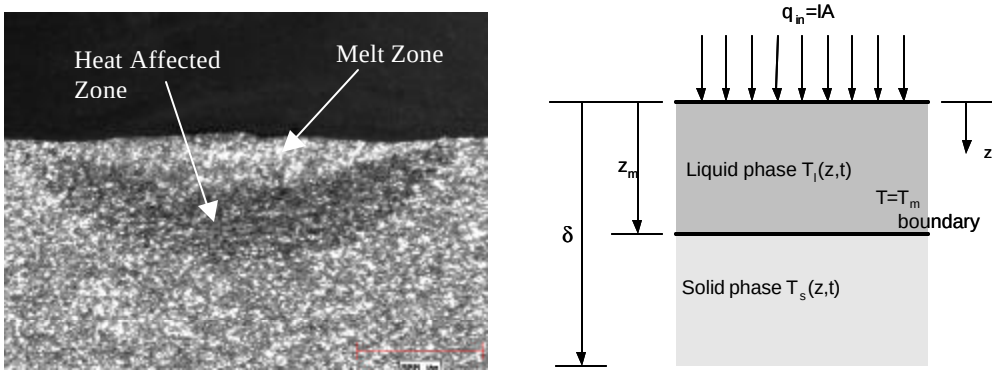

Figure 3: a) Cross section of low carbon steel test specimen scanned at Power = 1.1 kW and Vs = 11 m/min. b) Schematic diagram of one–dimensional moving phase boundary problem.

Heat diffusion equations:

$$\frac{\partial^2 T_l}{\partial z^2} = \frac{1}{a_l}\frac{\partial T_l}{\partial t} \qquad \text{Liquid Phase} \qquad (6a)$$

$$\frac{\partial^2 T_s}{\partial z^2} = \frac{1}{a_s}\frac{\partial T_s}{\partial t} \qquad \text{Solid Phase} \qquad (6b)$$

Boundary conditions:

$$-k_l \frac{\partial T_l}{\partial x} = AI \text{ at } z = 0 \qquad \text{Surface Heat Flux} \qquad (7)$$

$$k_s \frac{\partial T_s}{\partial x} - k_l \frac{\partial T_l}{\partial x} = rL\dot{z}_m(t) \qquad \text{Melt Interface Condition} \qquad (8)$$

$$T_l(z,t) = T_s(z,t) = T_m \text{ at } z = z_m(t) \qquad (9a)$$

$$T_s(\infty, t) = T_0 \qquad (9b)$$

$$T_s(z, t_0) = T_0 \qquad (9c)$$

1-D Approximate Integral Model

The approximate integral model was derived using the heat-balance integral solution method. [2] The heat-balance integral is the integral with respect to the space variable of the heat conduction equations. As a result Eqs. (6a) and (6b) become Eqs. (10a) and (10b) shown below. There are two moving boundaries: the melt depth and the thermal boundary layer thickness (see Figure 3b).

$$\left.\frac{\partial T_l}{\partial z}\right|_{z_m} - \left.\frac{\partial T_l}{\partial z}\right|_0 = \frac{1}{a_l}\frac{d}{dt}\left[\int_0^{z_m} T_l dz - \left(T_m\, z\big|_{z_m} - T_l\, z\big|_0\right)\right] \qquad (10a)$$

$$\left.\frac{\partial T_s}{\partial z}\right|_d - \left.\frac{\partial T_s}{\partial z}\right|_{z_m} = \frac{1}{a_s}\frac{d}{dt}\left[\int_{z_m}^{d} T_s dz - \left(T_0\, z\big|_d - T_m\, z\big|_{z_m}\right)\right] \qquad (10b)$$

Solutions were obtained by first assuming the temperature profiles were second order polynomial functions in the space variable, z and fit the given boundary conditions. Next, the profiles were substituted into Eqs. (10a), (10b), and (8). The result was three first order ODE's. The temperature profiles are given in Eqs. (14) and (15) shown below. The first order ODE's are shown below as Eqs. (16) – (18).

Before Melting: $0 \le t \le t_m$

$$T_s(z,t) = T_0 + \frac{AI}{2k_s d^2}\left[z - d\right]^2, 0 \le z \le d \qquad (11)$$

$$d = \sqrt{6a_s t} \qquad (12)$$

$$t_m = \frac{3k_s^2 (T_m - T_0)^2}{4a_s A^2 I^2} \qquad (13)$$

During Melting: $t_m \le t \le \Delta t$

$$T_l(z,t) = T_m + \left(2\,l\,z_m - \frac{AI}{k_l}\right)\left[z - z_m\right] + l\left[z - z_m\right]^2,\ 0 \le z \le z_m \quad (14)$$

$$T_s(z,t) = T_0 + \frac{(T_m - T_0)}{(z_m - d)^2}\left[z - d\right]^2,\ z_m \le z \le d \quad (15)$$

Eq. 16 is the state equation for the melt depth.

$$\dot{z}_m = \frac{AI}{\rho L} - \frac{2k_l\,l\,z_m}{\rho L} + \frac{2k_s\,(T_m - T_0)}{\rho L\,(z_m - d)} \quad (16)$$

Eq. 17 is the state equation for the thermal boundary layer thickness.

$$\dot{d} = -\frac{6\alpha_s}{(z_m - d)} - \frac{2AI}{\rho L} + \frac{4k_l\,l\,z_m}{\rho L} - \frac{4k_s\,(T_m - T_0)}{\rho L\,(z_m - d)} \quad (17)$$

Eq. 18 is the state equation for the coefficient in the liquid region temperature profile.

$$\dot{l} = \frac{3}{2z_m^2}\left(\frac{AI}{k_l} - 2\,l\,z_m\right)\left(\frac{AI}{\rho L} - \frac{2k_l\,l\,z_m}{\rho L} + \frac{2k_s\,(T_m - T_0)}{\rho L\,(z_m - d)}\right) - \frac{3\alpha_l\,l}{z_m^2} \quad (18)$$

The difference between this solution and classic solution is the assumption is not made that the moving boundaries are only functions of time. Goodman and others use the assumptions, $z_m = b\sqrt{\alpha t}$ and $d = g\sqrt{\alpha t}$, to reduce the solution to one independent variable, t.[2] The advantage of obtaining first order ODE's is MIMO control schemes can be readily implemented. Figure 4 shows the temperature distribution as a function of depth and time calculated using the approximate integral model. The dark line indicates the melting interface.

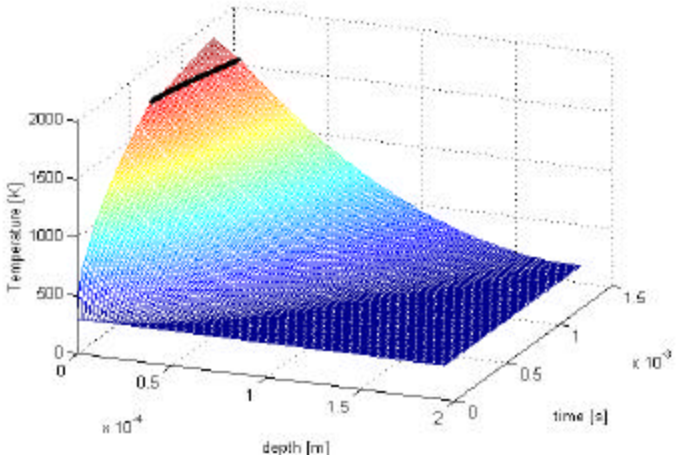

Figure 4: Simulation of 1-D melting using approximate integral model. Power = 230 W, V_s= 0.3 m/s, T_0 = 300K.

Xie & Kar's Model

Based on Sharma and et al.'s an approximate solution for one-dimensional phase-change heat conduction with time-dependent surface temperature [3], Xie and Kar [8] solved the one-dimensional phase-change with heat flux problem given by Eq. (6) by assuming a temperature distribution that satisfies the boundary and interface conditions (7)-(9). For liquid region, they assume a temperature profile which satisfies boundary conditions (7) and (9a) as follows,

For $0 \le z \le z_m(t)$:

$$T_l(z,t) = T_m - \frac{AI}{k_l}\left[z - z_m(t)\right] + \frac{AI}{2a_l k_l\left[1 + \frac{z_m(t)}{a_l}\dot{z}_m(t)\right]}\dot{z}_m(t)\left[z^2 - z_m{}^2(t)\right] \qquad (19)$$

In the solid region, they assume a temperature profile that satisfies boundary conditions (9), that is:

For $z > z_m(t)$:

$$T_s(z,t) = T_m - (T_m - T_0)\left\{1 - \exp\left[-\frac{1}{a_s}\dot{z}_m(t)(z - z_m(t))\right]\right\} \qquad (20)$$

The melt depth velocity is given below in Eq. 21.

$$\dot{z}_m(t) = \frac{2AI}{r\left[C_p(T_m - T_0) + L\right]\left\{1 + \sqrt{1 + \frac{4AIz_m(t)}{a_l r\left[C_p(T_m - T_0) + L\right]}}\right\}} \qquad (21)$$

The time for the surface to reach the melting temperature, t_m, is given by Eq. 22. [7]

$$t_m = \frac{p\,k_s{}^2(T_m - T_i)^2}{4a_s(AI)^2} \qquad (22)$$

The time required to reach the vaporization temperature, $t_{m\to v}$, can be calculated by using Eq.(21). The melt time, t_m, and the vaporization time, t_v, are used to establish upper and lower bounds on the interaction time, Δt.

Heat ablation model with heat input as function of absorption coefficient and melt depth

Based on the approximation solution for transient heat conduction by Zien [4] and Vujanovic [6], Beaman applied the solution to a vacuum arc remelting model.[10] Here by assuming heat flux is a function of melt depth the model can be applied to the laser melting process.

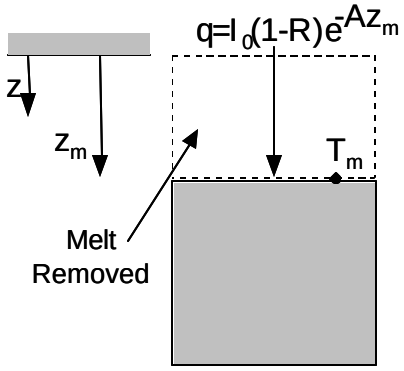

Figure 5: Schematic diagram of one–dimensional heat ablation problem.

The resulting equations are shown below as Eqs. (23) – (26).

$$\frac{dr}{dt} = \frac{C_{dd}\alpha_r}{d} - \frac{C_{dp}}{h_m} I(1-R)e^{-Az_m} \qquad (23)$$

$$\frac{dz_m}{dt} = -\frac{C_{sd}\alpha_r}{d} + \frac{C_{sp}}{h_m} I(1-R)e^{-Az_m} \qquad (24)$$

where:

$$C_{dp} = \frac{32\Lambda^*}{3\Lambda^* + 11} \qquad (25a)$$

$$C_{sp} = \frac{11\Lambda^*}{3\Lambda^* + 11} \qquad (25b)$$

$$C_{sd} = \frac{56\Lambda^*}{3\Lambda^* + 11}\left(\frac{1}{2} + \frac{b u_m}{3}\right) \qquad (25c)$$

$$C_{dd} = \frac{224(\Lambda^* + 1)}{3\Lambda^* + 11}\left(\frac{1}{2} + \frac{b u_m}{3}\right) \qquad (25d)$$

$$\Lambda^* = \frac{u_m}{u_{sup} - u_m} \qquad (26)$$

Experimental Setup

Experimental specimens were processed using a 1.1 kW CO_2 laser (beam diameter = .4 mm) operated in CW mode. The specimen was placed in vacuum chamber that was evacuated and back filled with argon to prevent oxidation. The power range used was 460 W to 1100 W. Multiple scan speeds were used at each power level to provide a range of interaction times to be compared to simulated results. The laser-scanning program utilizes a raster scan pattern shown in Fig. 7. In Fig. 7, w, L, V_t, and V_s are the scan track width, scan track length, transverse velocity, and scan velocity, respectively. The scan velocity, V_s, was difficult to measure directly, so it was calculated using Eq. 27 shown below. Here S_l is scanning density or scan lines per unit length.

$$V_s = \frac{wV_t}{L} S_l \qquad (27)$$

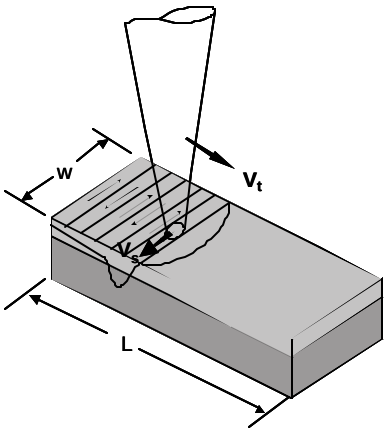

Figure 6: Raster scanning pattern of the 1.1 kW CO_2 laser.

The material used in the experiments was low carbon steel coated with graphite paint to increase the absorptivity of the samples. Two examples of the results are shown in Fig. 7. After processing, the samples were cut, grinded, polished, etched and measured using an optical microscope. The sample in Fig. 7a had the largest melt depth and the sample in Fig 7b had the least.

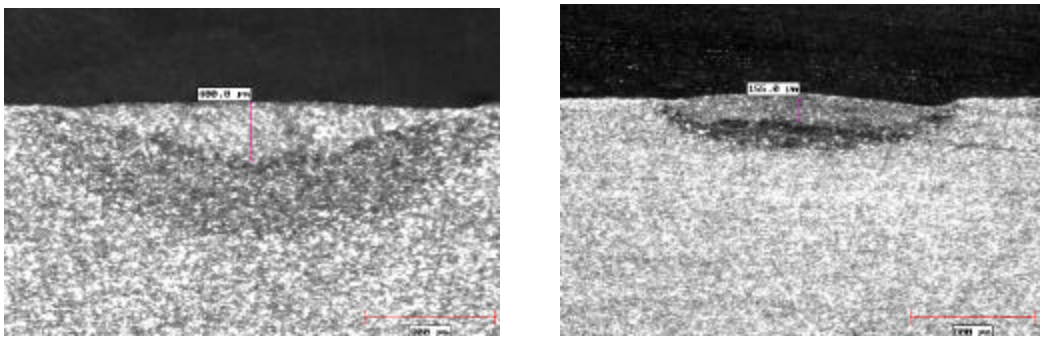

Figure 7: a) Scan track cross section of low carbon steel scanned at Power = 1100 W, Vs = 8 m/min, and melt depth ~ 400 µm. b) Scan track cross section of low carbon steel scanned at Power = 460 W, Vs = 21 m/min, and melt depth ~ 155 µm.

Results and Discussion

The experiments were conducted at three specific power levels: 1100 W, 715 W, and 460 W. The measurements taken from the experimental samples were plotted against the simulated results from all three models. Figures 8 through 10 show the results. The experimental points are indicated by points with error bars protruding. The error in melt depth measurement indicated by the error bars was estimated to be about 10 percent.

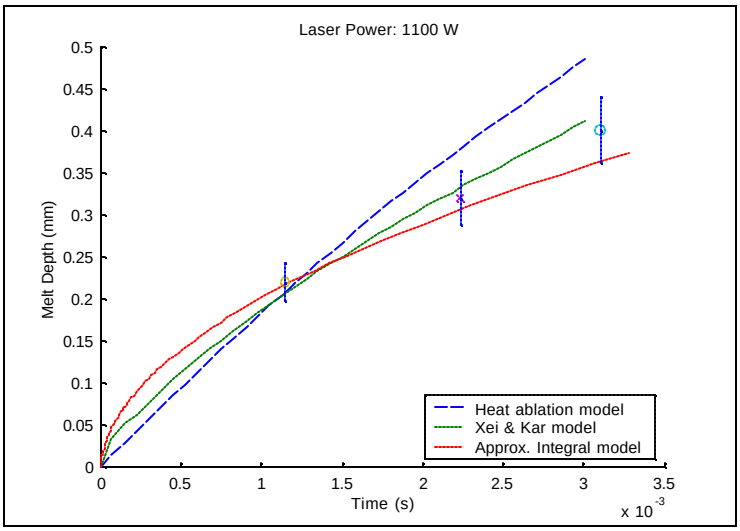

Figure 8: Melt Depth versus Interaction Time. Power = 1100 W.

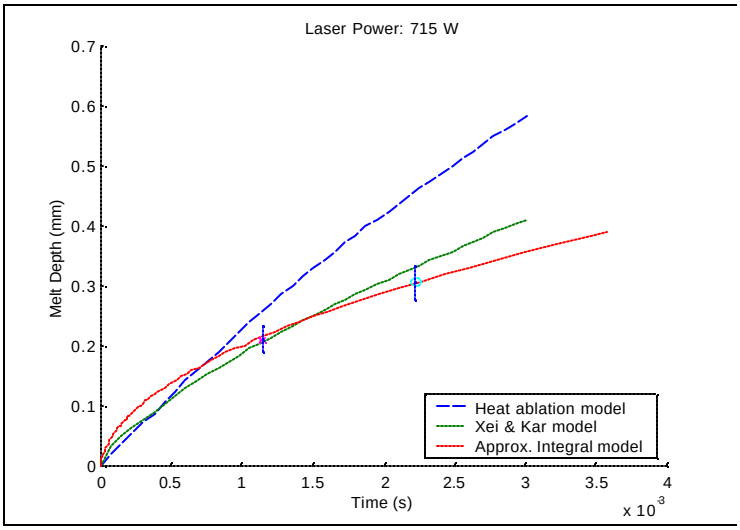

Figure 9: Melt Depth versus Interaction Time. Power = 715 W.

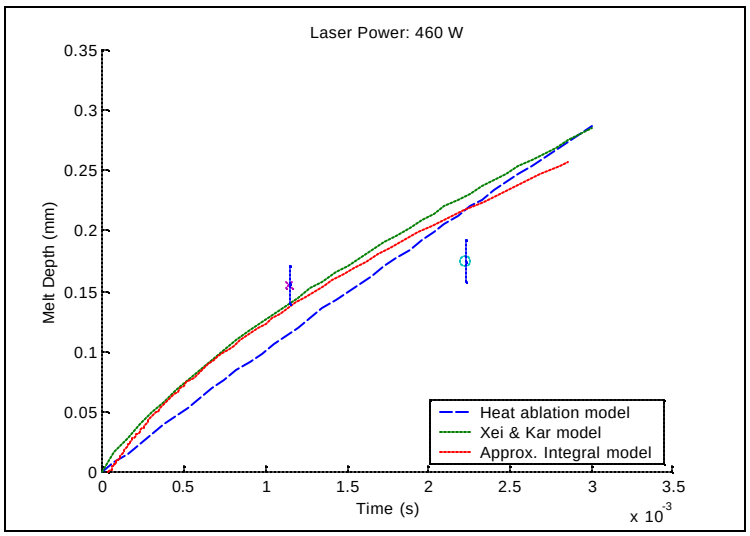

Figure 10: Melt Depth versus Interaction Time. Power = 460 W.

Both the Xie and Kar's model and the approximate integral model matched the experimental data well. The heat ablation model overestimates the melt depth as the interaction time increases. The simulated melt depths are highly sensitive to changes in absorption coefficient, so careful calibration must be performed to ensure proper performance. More accurate absorption coefficient data is needed for that process.

All three models can by used for control purposes, but the approximate integral model is more appropriate for MIMO control design. Figure 12 shows a block diagram of a MIMO control design concept.

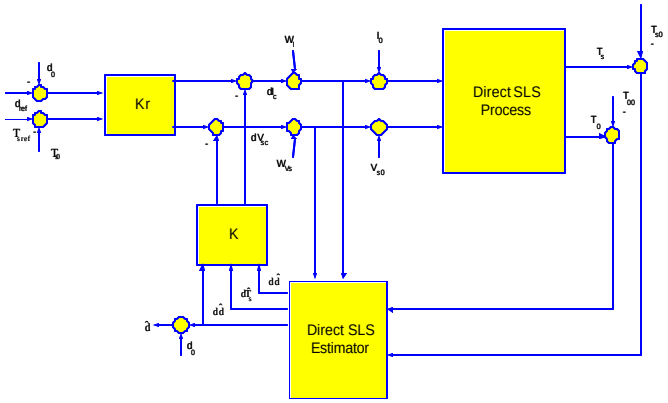

Figure 12: Block diagram of MIMO control design

Conclusions

The comparison between the experimental data and the simulations illustrates the conclusion that the 1-D Stefan problem provides a good approximation for the melt depth when the laser beam velocity is fast enough to make the interaction time less than the radial thermal diffusion time. The 1-D approximation solution can be fitted to the experimental data by adjusting the absorption coefficients of the solid and liquid regions. The models are highly sensitive to the absorptivities and more research must be done to determine how heat losses and material properties affect the overall absorption coefficients. Also for Direct SLS applications, density change during melting of powder-bed will be considered.[12]. Lastly, the approximate integral solution will be investigated further. The solution includes first order ODE's that easily can be adapted to MIMO control design. The design and implementation of the controller will be the future work and final goal of the research.

References

1. S. Das, *Direct selective laser sintering of high performance metals-machine design, process development and process control*, Ph.D Dissertation, The University of Texas at Austin, 1998.
2. T. R. Goodman and J. J. Shea, *The melting of finite slabs*, Journal of Applied Mechanics, Vol.27, pp.16-24, 1960.
3. O. P. Sharma, M. Rotenberg, and S. S. Penner, *Phase-change problems with variable surface temperature*, AIAA Journal, Vol.5, No.4, pp.667-682,1967.
4. T. F. Zien, *Integral solutions of ablation problems with time-dependent heat flux*, AIAA Journal Vol.16, No.12, pp.1287-1295, 1978.
5. M. N. Özisik, *Heat Conduction*, Wiley, New York, 1980.
6. B. D. Vujanovic and S. E. Jones, *Approximate solutions of canonical heat conduction equations*, Transactions of ASME, Vol.112, pp.836-842, 1990.
7. F. P. Incropera and D. P. DeWitt, *Fundamentals of Heat and Mass Transfer*, Wiley, New York, 1990.

8. J. Xie and A. Kar, *Mathematical modeling of melting during laser materials processing*, J. Appl. Phys., Vol.81, No.7, pp.3015-3022, 1997.
9. A. A. Rostami and A. Raisi, *Temperature distribution and melt pool size in a semi-infinite body due to a moving laser heat source*, Numerical Heat Transfer, Part A, Vol.31, pp.783-796, 1997.
10. D. K. Melgaard,R. L. Williamson, J.J. Beman, *Controlling remelting processes for superalloys and aerospace Ti alloys*, JOM, Vol.50, No.3, 1998.
12. Y. Zhang, A Faghri, *Melting of subcooled mixed powder bed with constant heat flux heating*, Int. J. Heat and Mass transfer, Vol.42 , pp.775 -788, 1999.
13. N.Jebbari, M. Jebari, F. Ahdad, A. Tarrats-Saugnac, J. P. Longuemard, *Energy mechanism during machining process by high-power continuous CO_2 laser*, Appl. Phys. B Vol.70(1), pp. 99-103, 1999.